

Lapeira, E., Mialdun, A., Yasnou, V. *et al.* Digital Interferometry Applied to Thermogravitational Technique. *Microgravity Sci. Technol.* **30**, 635–641 (2018).
<https://doi.org/10.1007/s12217-018-9632-7>

This version of the article has been accepted for publication, after peer review (when applicable) and is subject to Springer Nature's AM terms of use, but is not the Version of Record and does not reflect post-acceptance improvements, or any corrections. The Version of Record is available online at:

<https://doi.org/10.1007/s12217-018-9632-7>

1 DIGITAL INTERFEROMETRY APPLIED TO THERMOGRAVITATIONAL TECHNIQUE

2 E. Lapeira¹, A. Mialdun², V. Yasnou², P. Aristimuño¹, V. Shevtsova² and M. M. Bou-Ali¹3 ¹Mech. and Manufacturing Dept, MGEP Mondragon Goi Eskola Politeknikoa, Loramendi 4 Apdo. 23, 20500 Mondragon,
4 Spain5 ²MRC, CP165/62, Université Libre de Bruxelles, Av. F.D. Roosevelt, 50, B-1050, Brussels, Belgium

6

7 **Abstract**

8 In this work, we have applied Optical Digital
9 Interferometry approach to
10 thermogravitational micro-column
11 technique.

12 By the new analysis, we examine the entire
13 height of the micro-column and determine the
14 complete concentration profile inside. The
15 measurements were carried out by two lasers
16 with different wavelength $\lambda=633nm$ and
17 $\lambda=470nm$. The system was validated with
18 binary subsystems of the THN-IBB-C12
19 ternary mixture at equal mass fractions. The
20 results were compared with values of
21 Benchmark Fontainebleau and they showed
22 an excellent agreement.

23 **Keywords:** Thermodiffusion, binary
24 mixtures, Thermogravitational micro-
25 column, Optical Digital Interferometry.

26 **1. Introduction**

27 Since over last decades, optical methods have
28 been widely used in the determination of
29 transport properties as the thermodiffusion,
30 molecular diffusion and Soret coefficients of
31 binary mixtures. For example, Optical Beam
32 Deflection (Kolodner et al. 1988; Zhang et al.
33 1996), Optical Digital Interferometry
34 (Mialdun and Shevtsova 2008) and Thermal
35 Diffusion Forced Rayleigh Scattering
36 (Wiegand et al. 2007; Wittko and Köhler
37 2003) have been used to analyse several
38 binary mixtures. All these optical methods
39 have demonstrated good sensitivity in
40 measurements.

41 Now the challenge is focused on ternary
42 mixtures, so many of these techniques have
43 been modified in order to analyse more

44 complex systems. As a result, nowadays
45 several instruments **such as** (Gebhardt et al.
46 2013) and (Mialdun et al. 2015) are able to
47 determine the transport properties of different
48 ternary mixtures using optical analysis
49 methods or by **samples** extraction (Larrañaga
50 et al. 2015).

51 Optical methods allow to work with small
52 sample volume because the measurements
53 are usually carried out in situ. **In the case of**
54 **biological substances, for instance, it is not**
55 **always easy or possible to obtain big samples.**
56 **The conventional thermogravitational**
57 **parallelepiped and cylindrical columns**
58 **(Larrañaga et al. 2015b; Urteaga et al. 2012)**
59 **need at least 30 ml of sample, so it is not**
60 **viable to analyse biological samples using**
61 **those techniques.** For this reason, a new
62 thermogravitational micro-column was
63 designed, constructed and validated in
64 Mondragon University (Naumann et al.
65 2012) in order to determine the
66 thermodiffusion coefficient purely by optical
67 method. The sample volume of this micro-
68 column is less than 50 μ l so it makes feasible
69 the investigation of expensive substances,
70 which cannot be obtained in large quantities.
71 The optical approach applied to the micro-
72 column, made possible to analyse the
73 **continuous** concentration profile in binary
74 mixtures between two points. Nevertheless,
75 by this analysis method (Naumann et al.
76 2012), the accuracy of determining the
77 vertical concentration gradient was not so
78 good because it analysed only two points of
79 the height of micro-column.

80 Thus, in this work we have changed the
81 configuration of the **installation instrument**
82 **by** applying the Digital Interferometry. **The**
83 **new configuration** enables the analysis of the
84 concentration profile over the height of the
85 micro-column. The system was validated

86 using binary mixtures of Benchmark
87 Fontainebleau (Platten et al. 2003).

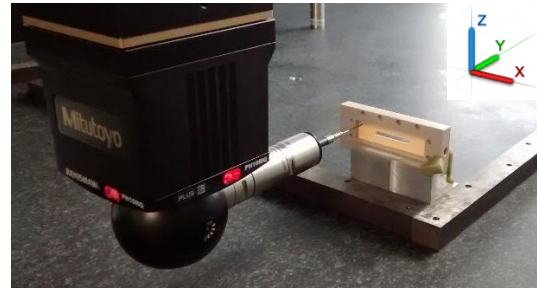
88 One of the benefits of this configuration is
89 that it measures the stationary separation in
90 situ without perturbing the mixture.
91 Therefore, it is going to be possible to analyse
92 the transitory theory of the
93 thermogravitational effect. In addition, it will
94 allow the convective stability analysis of
95 binary and ternary mixtures.

96 This article is organized as follows: in section
97 “Experimental setup”, a brief description of
98 the micro-column and the design of new
99 configuration of the optical arrangement and
100 image processing are explained. In section
101 “Results and discussion”, the results of
102 thermodiffusion coefficient of binary
103 mixtures are shown. Finally, section
104 “Conclusions” outlines the results.

105 2. Experimental setup

106 Thermogravitational micro-column

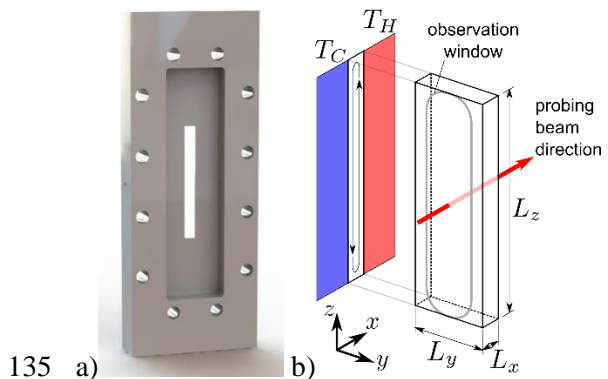
107 The thermogravitational micro-column used
108 in this work is the same as in (Naumann et al.
109 2012) with a slight difference. Only the core
110 part of the cell, shaping the gap of the micro-
111 column, was replaced for the reason that the
112 inlet and outlet were clogged up after
113 multiple uses. Therefore, we improved the
114 design to solve the problem. The new core
115 part was made with the same material Ketron
116 PEEK and was manufactured in Denatek
117 Engineering and Manufacturing
118 Technologies company with the greatest
119 accuracy possible. After the manufacturing
120 process, the gap size was verified in
121 Mondragon University by MITUTOYO
122 CRYSTA APEX S-7106 precision
123 coordinate measuring machine see Fig.1.



124

125 Fig.1 Measurement of the gap with MITUTOYO
126 CRYSTA APEX S-7106 machine.

127 The measurements with this machine consists
128 on selecting several points near the gap
129 Fig.2a on surface 1 and then changing Y axis,
130 selecting other points in surface 2, Fig.2b.
131 Finally, the distances between selected points
132 are calculated. The new gap thickness is
133 $L_x=0.51\pm 0.025$ mm, the height of $L_z=30$ mm
134 and width of $L_y=3$ mm.



135 a)

136 Fig.2 Core part of the micro-column, a) Shape of the
137 gap of the micro-column, b) Configuration of the gap.

138 Design of the new configuration of optical 139 diagnostics

140 The new configuration of the installation is
141 based on Digital Interferometer (Mialdun and
142 Shevtsova 2011). The two main contributions
143 of this configuration are: On the one hand, all
144 the height of the column is analysed as the
145 laser beam was expanded to cover all the
146 window of micro-column. On the other hand,
147 we introduced two lasers with different
148 wavelengths, a Diode-Pumped one with
149 $\lambda = 470\text{nm}$ wavelength (Spectra-Physics)
150 Fig.3 (1) and a He-Ne laser with $\lambda = 633\text{nm}$
151 wavelength (Research Electro-Optics) to be
152 able to analyse also ternary mixtures in the
153 future; below in this section the all notations
154 refer to Fig.3. In order to work with both
155 lasers at the same time without mixing their

156 interference patterns, we have designed a
 157 special shutter system that is installed at the
 158 exit aperture of each laser. This shutter
 159 system consists of a shaft moving up and
 160 down (3) allowing or denying the pass of
 161 **laser beam**. The movements of interrupter's
 162 shaft and the acquisition of images are
 163 synchronized by program implemented in
 164 LabView (8).

165 After the shutting system, both laser beams
 166 are passed ~~from~~ **through** neutral density
 167 filters in order to adjust the intensity Fig.3 (4).
 168 Then, to expand the beams, we used two
 169 spatial filter systems (Thorlab, KT310) with
 170 an aspheric lens, a pinhole and a collimator in
 171 order to obtain a good quality beam (5).
 172 Taking into account that the height of the
 173 micro-column is 30 mm, the final beam
 174 diameters were expanded to approximately
 175 40 mm. Afterwards, both **laser beams** are
 176 directed **into** a Mach-Zehnder interferometer
 177 (6), where each beam is divided into two
 178 equal beams. One passes through the micro-
 179 column (7) (object beam) and the other one is
 180 the reference beam. At the end of the
 181 interferometer, divided beams are joined
 182 creating an interference patterns that are
 183 acquired by CCD camera (QImaging
 184 QIClick-CCD Camera) (9).

185 Digital interferometry is a trusted technique
 186 that can be used to determine the
 208

187 concentration of a mixture **by** analysing the
 188 refractive index. The refractive index varies
 189 because of a temperature and concentration
 190 variations,

$$191 \quad \Delta n(y, z) = \left(\frac{\partial n}{\partial T} \right)_{T_o, c_o, \lambda} \Delta T(y, z) + \left(\frac{\partial n}{\partial c} \right)_{T_o, c_o, \lambda} \Delta c(y, z),$$

192

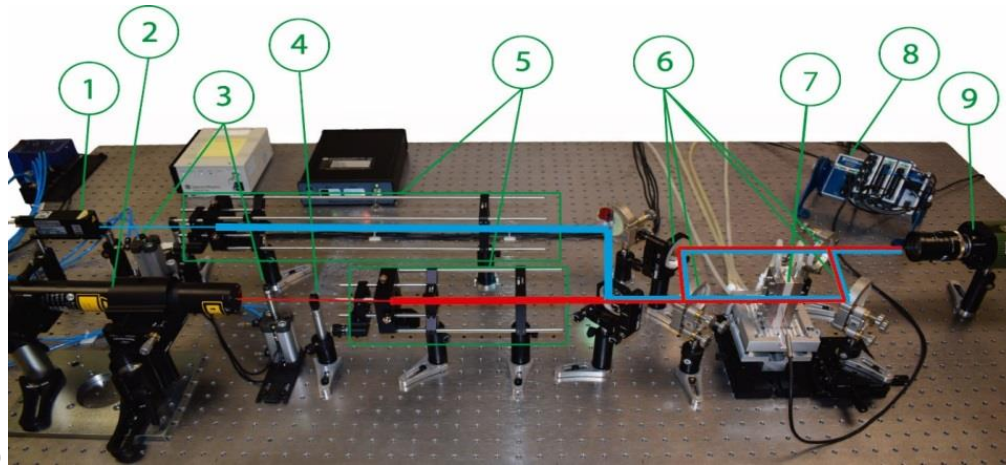
$$193 \quad (1)$$

194 Where, $(\partial n / \partial T)$ and $(\partial n / \partial c)$ are the contrast
 195 factors and $\Delta T(y, z)$ and $\Delta c(y, z)$ are the
 196 **spatial** temperature and concentration
 197 variations **in vertical direction**. In our system,
 198 the temperature gradient is applied in the
 199 same direction as the laser beam, so we can
 200 omit the temperature variation $\Delta T(y, z)$
 201 influence. Thus, the total variation of the
 202 refractive index is due to the concentration
 203 variation (2). In turn, Δn is obtained from the
 204 phase difference $\Delta \varphi$, which is measured by
 205 the interferometry (3), where L_x is the
 206 geometric path in liquid.

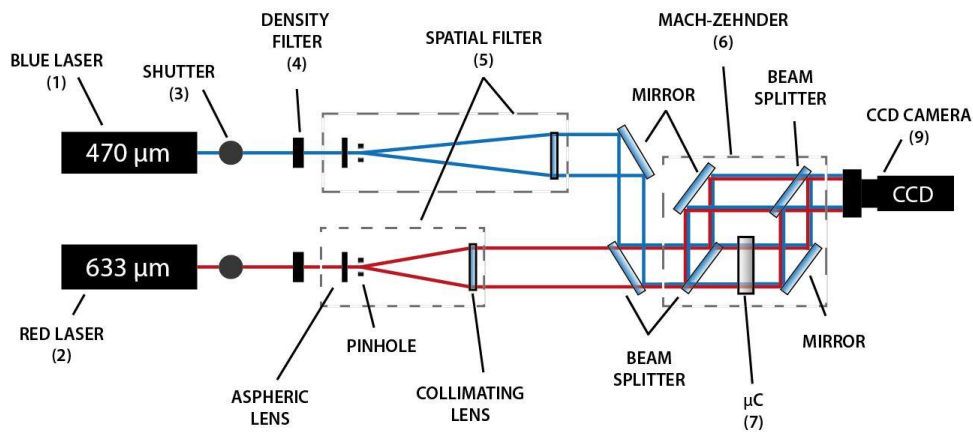
$$\Delta n(y, z) = \left(\frac{\partial n}{\partial c} \right)_{T_o, c_o, \lambda} \Delta c(y, z), \quad (2)$$

$$\Delta n(y, z) = \frac{\lambda}{2\pi L} \Delta \varphi(y, z) \quad (3)$$

207



209 a)



210 b)

211 Fig.3 Digital Interferometry applied to thermogravitational micro-column installation. a) Complete installation General view;
 212 b) Scheme of the installation.

213

214 **Experimental scenario and Image**
 215 **processing**

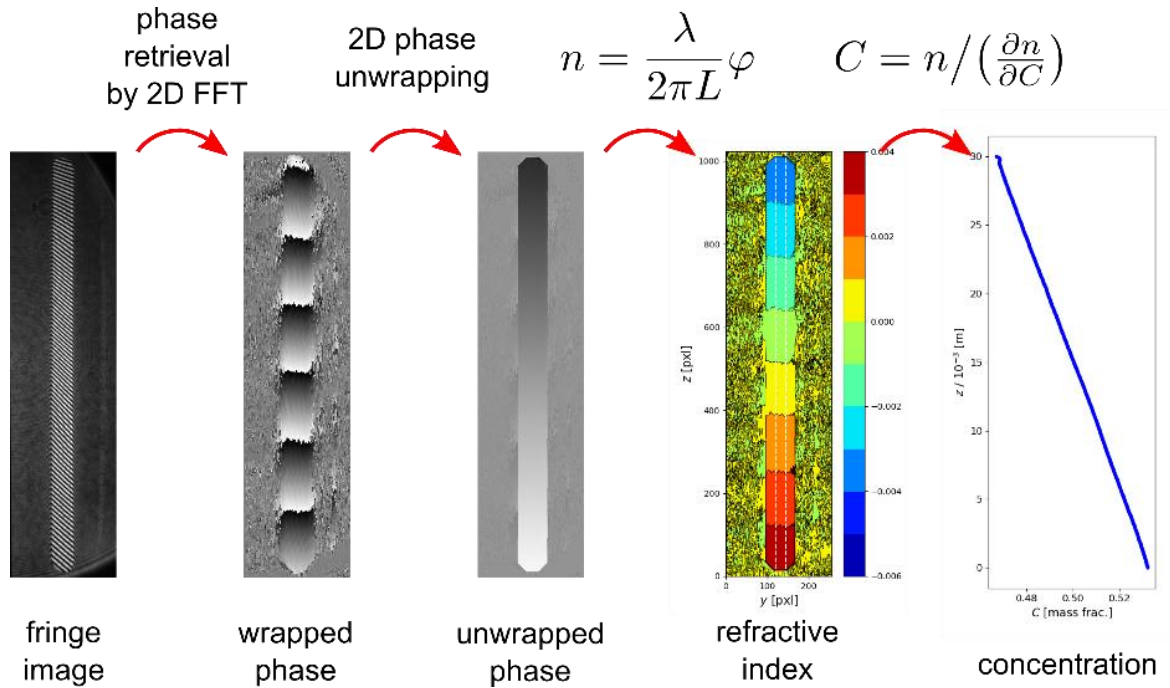
216 Both the interferometer configuration and
 217 image processing are based on Optical
 218 Digital Interferometry technique. Before
 219 starting the measurements, we stabilize the
 220 system at 25°C for 4 hours and acquire the
 221 images every 10 minutes in order to check the
 222 stability of the system. At the end of the
 223 measurement, one of the last acquired images
 224 in the stabilization step is taken as the
 225 reference image Fig.4. After applying the
 226 temperature gradient of $\Delta T = 8^\circ C$, the image
 227 acquisition rate is increased in order to see the
 228 evolution of phase variation in time. As the
 229 initial concentration change is bigger than
 230 near the stationary state, the acquisition of
 231 images is divided in three stages. For these
 232 binary mixtures, the image acquisition rate of
 233 first stage is 2 minutes during 36 minutes, in
 234 the second stage every 6 minutes during 72

235 minutes and finally every 12 minutes until the
 236 mixture reach the stationary state.

237 To extract the phase information from each
 238 acquired image, we use the 2D Fourier
 239 Transform technique described in literature
 240 (Mialdun and Shevtsova 2011). The Fig.4
 241 outlines the image analysis steps. The phase
 242 information enables the determination of the
 243 refractive index of the sample. As a result,
 244 knowing the concentration derivative of the
 245 refractive index ($\partial n / \partial c$) is possible to
 246 determine the entire concentration profile
 247 along the micro-column for each instant (for
 248 each acquired image). Once the mixture reach
 249 the stationary stage, the slope of the
 250 concentration along the height of the micro-
 251 column ($\partial c / \partial z$) is used in order to determine
 252 the thermodiffusion coefficient.

253 This concentration profile correspond to the
 254 midline of y scale of the column in y-z plane
 255 (bounded by white dashed lines in Fig.4).

256



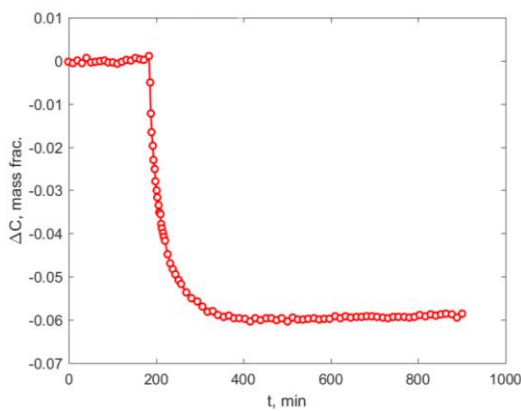
257

258

Fig.4 Steps for the phase information extraction of each acquired image.

259

260 The concentration variation during the all
 261 experiment is shown in Fig.5. There it can be
 262 appreciate the stabilization process at 25°C
 263 for approximately 3-4 hours. Then, the
 264 temperature gradient is applied so
 265 concentration in the sample start changing
 266 until mixture reach the stationary state.
 267 Negative concentration variation means that
 268 the reference component is enriched at the
 269 bottom part of the micro-column.



270

271 Fig.5 Separation of the concentration in time for
 272 measurement Time evolution of the concentration
 273 separation of THN-C12 binary mixture at 50% of mass
 274 fraction with $\Delta T = 8^\circ C$, monitored by and using
 275 470nm wavelength.

276 3. Results and discussion

277 For the validation of the new analysis
 278 method, we have measured the
 279 thermodiffusion coefficients of three binary
 280 mixtures at equal mass fraction of THN
 281 (purity, 98+%), IBB (purity, 99%) and C12
 282 (purity, 99%). All measurements have been
 283 carried out at mean temperature of 25°C. The
 284 thermophysical properties as density, thermal
 285 expansion and dynamic viscosity were taken
 286 from (Alonso de Mezquia et al. 2015) and the
 287 contrast factor $(\partial n / \partial c)$ at 633 nm
 288 wavelength of three binary mixtures were
 289 was taken from (Gebhardt et al. 2013). To
 290 calculate the $(\partial n / \partial c)$ at 470 nm, Cauchy
 291 dispersion relation has been used as it is
 292 detailed in (Mialdun, A. and Shevtsova
 293 2017). In Table 1, all the optical and
 294 thermophysical properties taken from
 295 literature are shown.

296

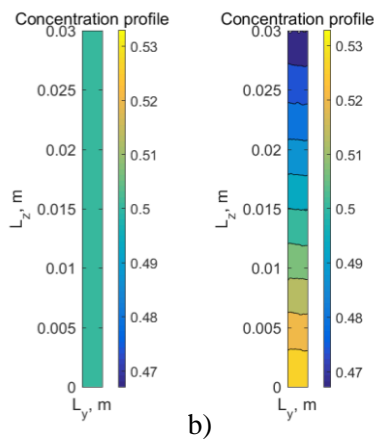
297

298 Table 1. Optical and thermophysical properties of
 299 THN-IBB-C12 binary mixtures at equal mass fraction
 300 at 25°C. Density, thermal expansion and dynamic
 301 viscosity are taken from (Alonso de Mezquia et al.
 302 2015) and $(\partial n/\partial c)$ from (Gebhardt et al. 2013).

	THN- C12	THN- IBB	IBB- C12
ρ (kg/m^3)	841.248	904.514	792.355
$\alpha \times 10^{-3}$ (K^{-1})	0.895	0.888	0.961
$\mu \times 10^{-3}$ ($Pa s$)	1.523	1.374	1.133
$(\partial n/\partial c)$ ($\lambda = 633nm$)	0.1155	0.0547	0.0625
$(\partial n/\partial c)$ ($\lambda = 470nm$)	0.1258	0.0577	0.0700

303

304 During the image processing, the
 305 concentration in the entire cross-section of
 306 the cell is determined ~~in~~ from each image.
 307 The Fig.6a shows the initial concentration
 308 profile when the micro-column is stabilized
 309 at 25°C and in Fig.6b when it reaches the
 310 stationary state with $\Delta T = 8^\circ C$.

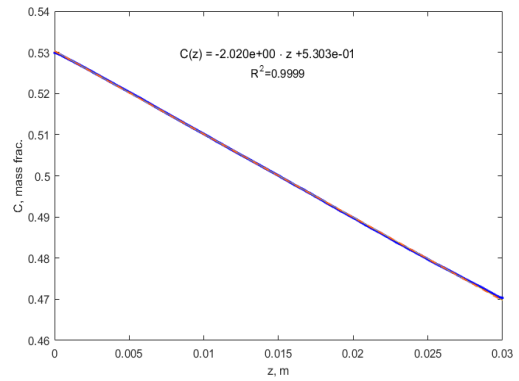


311 a)

b)

312 Fig.6 Concentration profiles inside the micro-column ~~of~~
 313 filled with THN-C12 at 50 % mass fraction; a) when
 314 mixtures is stabilized at 25° C , b) when the mixtures
 315 reaches the stationary state after applying $\Delta T = 8^\circ C$.

316 Afterwards, the vertical concentration profile
 317 is represented in function of the height of the
 318 micro-column and is fitted with the
 319 polynomial of the first order obtaining
 320 $(\partial c/\partial z)$ as shown in Fig.7.



321

322 Fig.7 Concentration gradient at stationary state along
 323 the height of the micro-column of THN-C12 at 50%
 324 mass fraction with $\Delta T = 8^\circ C$.

325 Finally, the thermodiffusion coefficient of
 326 binary mixtures is determined (4) (Larrañaga
 327 et al. 2014),

$$D_T = -\frac{L_x^4}{504} \frac{g \alpha}{\nu C_0 (1 - C_0)} \frac{\partial c}{\partial z} \quad (4)$$

328 where, L_x is the gap of the micro-column, g
 329 is the gravity, α is the thermal expansion
 330 coefficient, ν is the kinematic viscosity and
 331 C_0 is the initial concentration of the
 332 reference component.

333 The Table 2, Table 3 and Table 4 show the
 334 thermodiffusion coefficients of THN-C12,
 335 THN-IBB and IBB-C12 binary mixtures and
 336 the mean values with the respective
 337 deviations.

338 The obtained results show a good agreement
 339 with Benchmark Fontainebleau values
 340 (Platten et al. 2003) ~~so we have seen that the~~
 341 ~~new configuration provides reliable results~~
 342 ~~that makes us confident in reliability of the~~
 343 ~~new configuration.~~

344 For the first time, with the new
 345 configuration, we have analysed all the
 346 height of the column and we have seen the
 347 entire concentration profile inside the
 348 thermogravitational column.

349 Table 2. Thermodiffusion coefficients of THN-C12 binary mixtures at 50% mass fraction.

THN-C12	633 nm		470 nm		Benchmark (Platten et al. 2003)
	$(\partial c/\partial z)$	$D_T \times 10^{-12}$ (m^2/sK)	$(\partial c/\partial z)$	$D_T \times 10^{-12}$ (m^2/sK)	
1	-2.124	5.53	-2.070	5.39	
2	-2.264	5.90	-2.177	5.66	
3	-2.304	5.99	-2.275	5.92	
4	-2.260	5.88	-2.180	5.68	
5	-2.299	5.99	-2.212	5.76	
Average	-2.250	5.86±0.33	-2.183	5.68±0.29	5.9±0.3

350

351 Table 3. Thermodiffusion coefficients of THN-IBB binary mixtures at 50% mass fraction.

THN-IBB	633 nm		470 nm		Benchmark (Platten et al. 2003)
	$(\partial c/\partial z)$	$D_T \times 10^{-12}$ (m^2/sK)	$(\partial c/\partial z)$	$D_T \times 10^{-12}$ (m^2/sK)	
1	-1.062	3.27	-1.010	3.11	
2	-0.801	2.46	-0.794	2.44	
3	-0.844	2.60	-0.804	2.68	
4	-1.062	3.27	-0.983	3.03	
5	-0.937	3.03	-0.984	2.89	
6	-0.902	2.78	-0.877	2.70	
Average	-0.935	2.90±0.44	-0.909	2.81±0.37	2.8±0.1

352

353 Table 4. Thermodiffusion coefficients of IBB-C12 binary mixtures at 50% mass fraction.

IBB-C12	633 nm		470 nm		Benchmark (Platten et al. 2003)
	$(\partial c/\partial z)$	$D_T \times 10^{-12}$ (m^2/sK)	$(\partial c/\partial z)$	$D_T \times 10^{-12}$ (m^2/sK)	
1	-1.079	3.82	-1.022	3.61	
2	-0.994	3.52	-0.987	3.49	
3	-1.209	4.28	-1.094	3.87	
4	-1.123	3.98	-1.074	3.80	
5	-1.146	4.06	-1.112	3.94	
6	-1.071	3.79	-0.988	3.49	
Average	-1.104	3.91±0.39	-1.046	3.70±0.24	3.7±0.2

354

355 4. Conclusions

356 In this work, we have changed the
 357 configuration of the **previously reported**
 358 **optical** analysis method applied to
 359 thermogravitational micro-column. The new
 360 configuration of the interferometer and the
 361 image processing is based on Optical Digital
 362 Interferometry analysis method. With the
 363 new configuration, we are able to analyse the
 364 entire window of micro-column instead of
 365 analysing only two points. Thanks to this
 366 **improvement**, we are able to see the entire
 367 concentration profile inside the micro-
 368 column during the measurements.

369 To validate the new system, we have
 370 determined the thermodiffusion coefficients
 371 of three binary mixtures at equal mass
 372 fractions. Results have been compared with
 373 Benchmark Fontainebleau

374 ~~By the~~The new analysis method ~~in future it is~~
 375 ~~going to be possible~~ can be readily extended
 376 to analyse ternary mixtures. The analysis of
 377 the entire concentration profile will allow to
 378 study the thermogravitational effect in the
 379 transitory state of binary and ternary
 380 mixtures.

381 Acknowledgements

382 Authors would like to thank the support of
383 Research Groups (IT1009-16) and Research
384 Fellowship (Pre_2014_1_283) of Basque
385 Government, TERDISOMEZ (FIS2014-
386 58950-C2-1-P) and MEZNAFLU (ESP2017-
387 83544-C3-1-P) of the MINECO and DCMIX
388 (DCMIX-NCR-00022-QS) from the
389 European Space Agency. Also would like to
390 thank Denatek engineering and
391 manufacturing technology company for
392 manufacturing the gap.

393 References

- 394 Alonso de Mezquia, D., Larrañaga, M., Bou-Ali,
395 M.M., Madariaga, J.A., Santamaría, C., Platten, J.K.:
396 Contribution to thermodiffusion coefficient
397 measurements in DCMIX project. *Int. J. Therm. Sci.*
398 92, 14–16 (2015).
399 doi:10.1016/j.ijthermalsci.2015.01.013
- 400 Gebhardt, M., Köhler, W., Mialdun, A., Yasnou, V.,
401 Shevtsova, V.: Diffusion, thermal diffusion, and Soret
402 coefficients and optical contrast factors of the binary
403 mixtures of dodecane, isobutylbenzene, and 1,2,3,4-
404 tetrahydronaphthalene. *J. Chem. Phys.* 138, 114503
405 (2013). doi:10.1063/1.4795432
- 406 Kolodner, P., Williams, H., Moe, C.: Optical
407 measurement of the Soret coefficient of ethanol/water
408 solutions. *J. Chem. Phys.* 88, 6512–6524 (1988)
- 409 Larrañaga, M., Bou-Ali, M.M., Lapeira, E.,
410 Santamaría, C., Madariaga, J.A.: Effect of
411 Thermophysical Properties and Morphology of the
412 Molecules on Thermodiffusion Coefficient of Binary
413 Mixtures. *Microgravity Sci. Technol.* 26, 29–35 (2014).
414 doi:10.1007/s12217-014-9368-y
- 415 Larrañaga, M., Bou-Ali, M.M., Lizarraga, I.,
416 Madariaga, J.A., Santamaría, C.: Soret coefficients of
417 the ternary mixture 1,2,3,4-tetrahydronaphthalene +
418 isobutylbenzene + n-dodecane. *J. Chem. Phys.* 143,
419 24202 (2015)(a). doi:10.1063/1.4926654
- 420 Larrañaga, M., Bou-Ali, M.M., Lizarraga, I.,
421 Madariaga, J.A., Santamaría, C.: Soret coefficients of
422 the ternary mixture 1,2,3,4-tetrahydronaphthalene +
423 isobutylbenzene + n-dodecane. *J. Chem. Phys.* 143,
424 24202 (2015)(b). doi:10.1063/1.4926654
- 425 Mialdun, A. and Shevtsova, V.: Analysis of multi-
426 wavelength measurements of diffusive properties via
427 dispersion dependence of optical properties. *Appl. Opt.*
428 56, 572–581 (2017)
- 429 Mialdun, A., Legros, J.-C., Yasnou, V., Sechenyh, V.,
430 Shevtsova, V.: Contribution to the benchmark for
431 ternary mixtures: Measurement of the Soret, diffusion
432 and thermodiffusion coefficients in the ternary mixture
433 THN/IBB/nC12 with 0.8/0.1/0.1 mass fractions in
434 ground and orbital laboratories. *Eur. Phys. J. E.* 38, 27
435 (2015). doi:10.1140/epje/i2015-15027-2

- 436 Mialdun, A., Shevtsova, V.: Measurement of the Soret
437 and diffusion coefficients for benchmark binary
438 mixtures by means of digital interferometry. *J. Chem.*
439 *Phys.* 134, 44524 (2011). doi:10.1063/1.3546036
- 440 Mialdun, A., Shevtsova, V.M.: Development of optical
441 digital interferometry technique for measurement of
442 thermodiffusion coefficients. *Int. J. Heat Mass Transf.*
443 51, 3164–3178 (2008).
444 doi:10.1016/j.ijheatmasstransfer.2007.08.020
- 445 Naumann, P., Martin, A., Kriegs, H., Larrañaga, M.,
446 Bou-Ali, M.M., Wiegand, S.: Development of a
447 thermogravitational microcolumn with an
448 interferometric contactless detection system. *J. Phys.*
449 *Chem. B.* 116, 13889–97 (2012).
450 doi:10.1021/jp3098473
- 451 Platten, J.K., Bou-Ali, M.M., Costesèque, P., Dutrieux,
452 J.F., Köhler, W., Leppla, C., Wiegand, S., Wittko, G.:
453 Benchmark values for the Soret, thermal diffusion and
454 diffusion coefficients of three binary organic liquid
455 mixtures. *Philos. Mag.* 83, 1965–1971 (2003).
456 doi:10.1080/0141861031000108204
- 457 Urteaga, P., Bou-Ali, M.M., Alonso De Mezquia, D.,
458 Santamaría, J., Santamaría, C., Madariaga, J.A.,
459 Bataller, H.: Measurement of thermodiffusion
460 coefficient of hydrocarbon binary mixtures under
461 pressure with the thermogravitational technique. *Rev.*
462 *Sci. Instrum.* 83, (2012). doi:10.1063/1.4737628
- 463 Wiegand, S., Ning, H., Kriegs, H.: Thermal diffusion
464 forced Rayleigh scattering Setup optimized for aqueous
465 mixtures. *J. Phys. Chem. B.* 111, 14169–14174 (2007).
466 doi:10.1021/jp076913y
- 467 Wittko, G., Köhler, W.: Precise determination of the
468 Soret, thermal diffusion and mass diffusion coefficients
469 of binary mixtures of dodecane, isobutylbenzene and
470 1,2,3,4-tetrahydronaphthalene by a holographic grating
471 technique. *Philos. Mag.* 83, 1973–1987 (2003).
472 doi:10.1080/0141861031000108213
- 473 Zhang, K.J., Briggs, M.E., Gammon, R.W., Sengers, J.
474 V.: Optical measurement of the Soret coefficient and
475 the diffusion coefficient of liquid mixtures. *J. Chem.*
476 *Phys.* 104, 6881 (1996). doi:10.1063/1.471355

477

1 DIGITAL INTERFEROMETRY APPLIED TO THERMOGRAVITATIONAL TECHNIQUE

2 E. Lapeira¹, A. Mialdun², V. Yasnou², P. Aristimuño¹, V. Shevtsova² and M. M. Bou-Ali¹3 ¹Mech. and Manufacturing Dept, MGEP Mondragon Goi Eskola Politeknikoa, Loramendi 4 Apdo. 23, 20500 Mondragon,
4 Spain5 ²MRC, CP165/62, Université Libre de Bruxelles, Av. F.D. Roosevelt, 50, B-1050, Brussels, Belgium

6

7 **Abstract**

8 In this work, we have applied Optical
9 Digital Interferometry approach to
10 thermogravitational micro-column
11 technique.

12 By the new analysis, we examine the entire
13 height of the micro-column and determine
14 the complete concentration profile inside.
15 The measurements were carried out by two
16 lasers with different wavelength $\lambda=633nm$
17 and $\lambda=470nm$. The system was validated
18 with binary subsystems of the THN-IBB-
19 C12 ternary mixture at equal mass fractions.
20 The results were compared with values of
21 Benchmark Fontainebleau and they showed
22 an excellent agreement.

23 **Keywords:** Thermodiffusion, binary
24 mixtures, Thermogravitational micro-
25 column, Optical Digital Interferometry.

26 **1. Introduction**

27 Since over last decades, optical methods
28 have been widely used in the determination
29 of transport properties as the
30 thermodiffusion, molecular diffusion and
31 Soret coefficients of binary mixtures. For
32 example, Optical Beam Deflection
33 (Kolodner et al. 1988; Zhang et al. 1996),
34 Optical Digital Interferometry (Mialdun and
35 Shevtsova 2008) and Thermal Diffusion
36 Forced Rayleigh Scattering (Wiegand et al.
37 2007; Wittko and Köhler 2003) have been
38 used to analyse several binary mixtures. All
39 these optical methods have demonstrated
40 good sensitivity in measurements.

41 Now the challenge is focused on ternary
42 mixtures, so many of these techniques have
43 been modified in order to analyse more

44 complex systems. As a result, nowadays
45 several instruments such as (Gebhardt et al.
46 2013) and (Mialdun et al. 2015) are able to
47 determine the transport properties of
48 different ternary mixtures using optical
49 analysis methods or by samples extraction
50 (Larrañaga et al. 2015).

51 Optical methods allow to work with small
52 sample volume because the measurements
53 are usually carried out in situ. In the case of
54 biological substances, for instance, it is not
55 always easy or possible to obtain big
56 samples. The conventional
57 thermogravitational parallelepiped and
58 cylindrical columns (Larrañaga et al. 2015b;
59 Urteaga et al. 2012) need at least 30 ml of
60 sample, so it is not viable to analyse
61 biological samples using those techniques.
62 For this reason, a new thermogravitational
63 micro-column was designed, constructed
64 and validated in Mondragon University
65 (Naumann et al. 2012) in order to determine
66 the thermodiffusion coefficient purely by
67 optical method. The sample volume of this
68 micro-column is less than 50 μ l so it makes
69 feasible the investigation of expensive
70 substances, which cannot be obtained in
71 large quantities. The optical approach
72 applied to the micro-column, made possible
73 to analyse the continuous concentration
74 profile in binary mixtures between two
75 points. Nevertheless, by this analysis method
76 (Naumann et al. 2012), the accuracy of
77 determining the vertical concentration
78 gradient was not so good because it analysed
79 only two points of the height of micro-
80 column.

81 Thus, in this work we have changed the
82 configuration of the instrument by applying
83 the Digital Interferometry. The new
84 configuration enables the analysis of the
85 concentration profile over the height of the

86 micro-column. The system was validated
87 using binary mixtures of Benchmark
88 Fontainebleau (Platten et al. 2003).

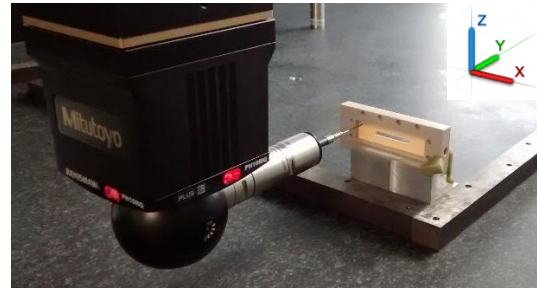
89 One of the benefits of this configuration is
90 that it measures the stationary separation in
91 situ without perturbing the mixture.
92 Therefore, it is going to be possible to
93 analyse the transitory theory of the
94 thermogravitational effect. In addition, it
95 will allow the convective stability analysis
96 of binary and ternary mixtures.

97 This article is organized as follows: in
98 section “Experimental setup”, a brief
99 description of the micro-column and the
100 design of new configuration of the optical
101 arrangement and image processing are
102 explained. In section “Results and
103 discussion”, the results of thermodiffusion
104 coefficient of binary mixtures are shown.
105 Finally, section “Conclusions” outlines the
106 results.

107 2. Experimental setup

108 Thermogravitational micro-column

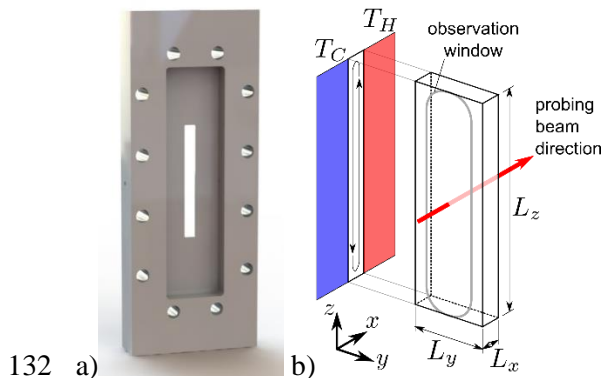
109 The thermogravitational micro-column used
110 in this work is the same as in (Naumann et
111 al. 2012) with a slight difference. Only the
112 core part of the cell, shaping the gap of the
113 micro-column, was replaced for the reason
114 that the inlet and outlet were clogged up
115 after multiple uses. Therefore, we improved
116 the design to solve the problem. The new
117 core part was made with the same material
118 *Ketron PEEK* and was manufactured in
119 *Denatek Engineering and Manufacturing*
120 *Technologies* company with the greatest
121 accuracy possible. After the manufacturing
122 process, the gap size was verified in
123 Mondragon University by MITUTOYO
124 CRYSTA APEX S-7106 precision
125 coordinate measuring machine see Fig.1.



126

127 Fig.1 Measurement of the gap with MITUTOYO
128 CRYSTA APEX S-7106 machine.

129 The new gap thickness is $L_x=0.51\pm 0.025$
130 mm, the height of $L_z=30$ mm and width of
131 $L_y=3$ mm.



132 a)

133 Fig.2 Core part of the micro-column, a) Shape of the
134 gap of the micro-column, b) Configuration of the gap.

135 Design of the new configuration of optical 136 diagnostics

137 The new configuration of the installation is
138 based on Digital Interferometer (Mialdun
139 and Shevtsova 2011). The two main
140 contributions of this configuration are: On
141 the one hand, all the height of the column is
142 analysed as the laser beam was expanded to
143 cover all the window of micro-column. On
144 the other hand, we introduced two lasers
145 with different wavelengths, a Diode-Pumped
146 one with $\lambda = 470\text{nm}$ wavelength (Spectra-
147 Physics) Fig.3 (1) and a He-Ne laser with
148 $\lambda = 633\text{nm}$ wavelength (Research Electro-
149 Optics) to be able to analyse also ternary
150 mixtures in the future; below in this section
151 the all notations refer to Fig.3. In order to
152 work with both lasers at the same time
153 without mixing their interference patterns,
154 we have designed a special shutter system
155 that is installed at the exit aperture of each
156 laser. This shutter system consists of a shaft
157 moving up and down (3) allowing or

158 denying the pass of laser beam. The
 159 movements of interrupter's shaft and the
 160 acquisition of images are synchronized by
 161 program implemented in LabView (8).

162 After the shutting system, both laser beams
 163 are passed through neutral density filters in
 164 order to adjust the intensity Fig.3 (4). Then,
 165 to expand the beams, we used two spatial
 166 filter systems (Thorlab, KT310) with an
 167 aspheric lens, a pinhole and a collimator in
 168 order to obtain a good quality beam (5).
 169 Taking into account that the height of the
 170 micro-column is 30 mm, the final beam
 171 diameters were expanded to approximately
 172 40 mm. Afterwards, both beams are directed
 173 into a Mach-Zehnder interferometer (6),
 174 where each beam is divided into two equal
 175 beams. One passes through the micro-
 176 column (7) (object beam) and the other one
 177 is the reference beam. At the end of the
 178 interferometer, divided beams are joined
 179 creating an interference patterns that are
 180 acquired by CCD camera (QImaging
 181 QIClick-CCD Camera) (9).

182 Digital interferometry is a trusted technique
 183 that can be used to determine the
 184 concentration of a mixture by analysing the

185 refractive index. The refractive index varies
 186 because of a temperature and concentration
 187 variations,

$$188 \quad \Delta n(y, z) = \left(\frac{\partial n}{\partial T} \right)_{T_o, c_o, \lambda} \Delta T(y, z) + \left(\frac{\partial n}{\partial c} \right)_{T_o, c_o, \lambda} \Delta c(y, z),$$

189
190 (1)

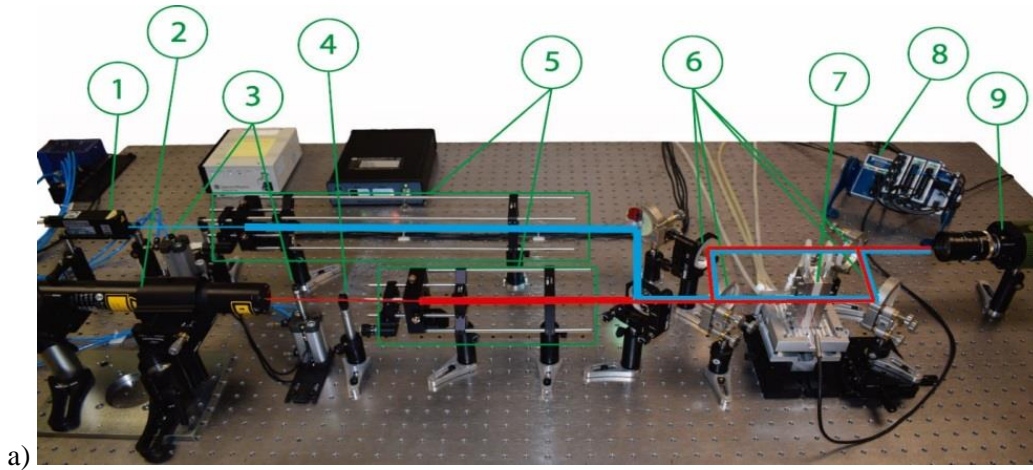
191 Where, $(\partial n / \partial T)$ and $(\partial n / \partial c)$ are the contrast
 192 factors and $\Delta T(y, z)$ and $\Delta c(y, z)$ are the
 193 spatial temperature and concentration
 194 variations. In our system, the temperature
 195 gradient is applied in the same direction as
 196 the laser beam, so we can omit the
 197 temperature variation $\Delta T(y, z)$ influence.
 198 Thus, the total variation of the refractive
 199 index is due to the concentration variation
 200 (2). In turn, Δn is obtained from the phase
 201 difference $\Delta \varphi$, which is measured by the
 202 interferometry (3), where L_x is the
 203 geometric path in liquid.

$$204 \quad \Delta n(y, z) = \left(\frac{\partial n}{\partial c} \right)_{T_o, c_o, \lambda} \Delta c(y, z), \quad (2)$$

$$\Delta n(y, z) = \frac{\lambda}{2\pi L} \Delta \varphi(y, z) \quad (3)$$

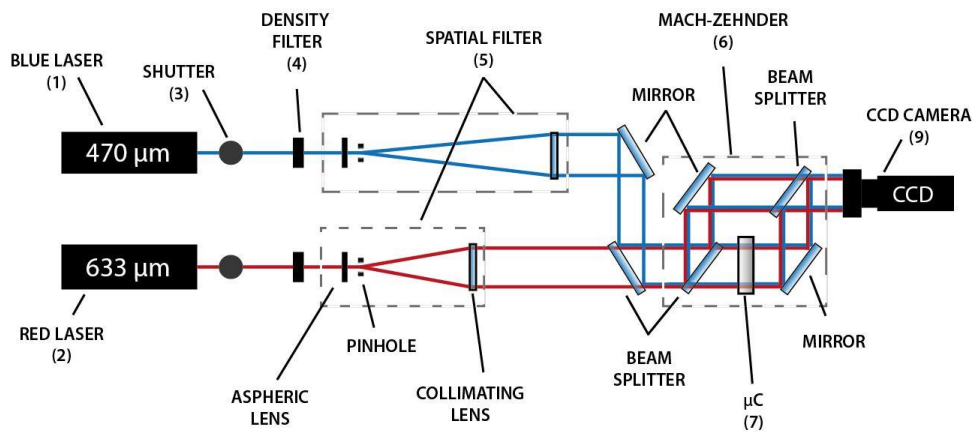
204

206



207

b)



208
209

Fig.3 Digital Interferometry applied to thermogravitational micro-column installation. a) General view; b) Scheme of the installation.

210

211 Experimental scenario and Image 212 processing

213 Both the interferometer configuration and
214 image processing are based on Optical
215 Digital Interferometry technique. Before
216 starting the measurements, we stabilize the
217 system at 25°C for 4 hours and acquire the
218 images every 10 minutes in order to check
219 the stability of the system. At the end of the
220 measurement, one of the last acquired
221 images in the stabilization step is taken as
222 the reference image. After applying the
223 temperature gradient of $\Delta T = 8^\circ C$, the image
224 acquisition rate is increased in order to see
225 the evolution of phase variation in time. As
226 the initial concentration change is bigger
227 than near the stationary state, the acquisition
228 of images is divided in three stages. For
229 these binary mixtures, the image acquisition
230 rate of first stage is 2 minutes during 36
231 minutes, in the second stage every 6 minutes

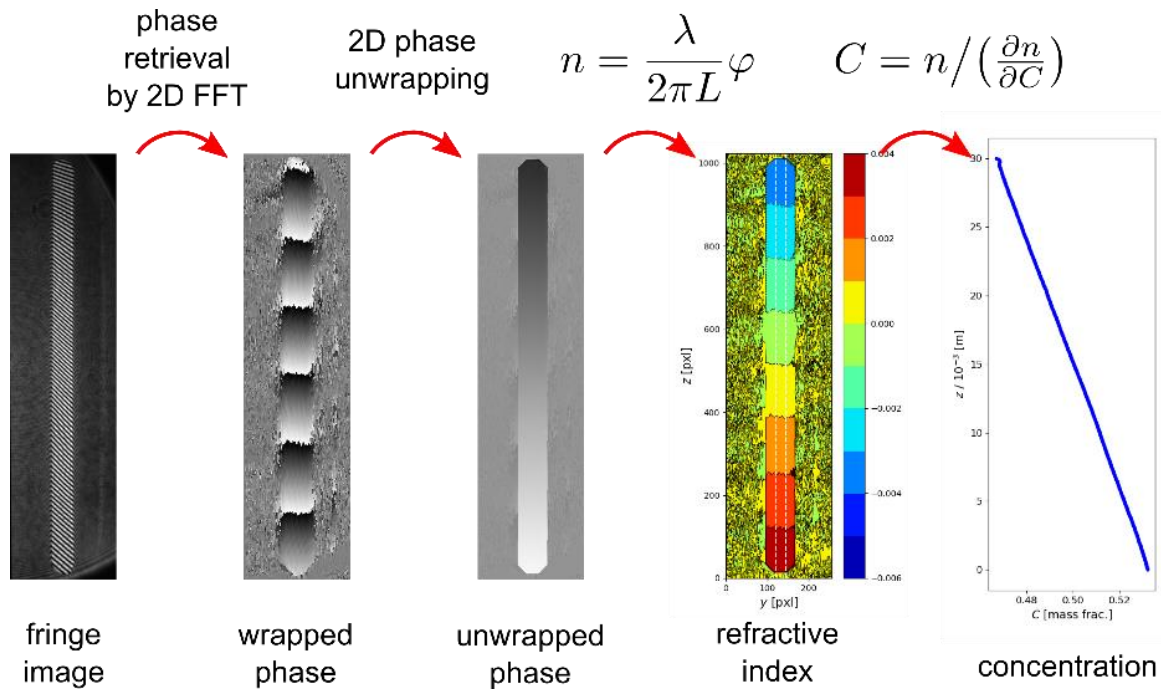
232 during 72 minutes and finally every 12
233 minutes until the mixture reach the
234 stationary state.

235 To extract the phase information from each
236 acquired image, we use the 2D Fourier
237 Transform technique described in literature
238 (Mialdun and Shevtsova 2011). The Fig.4
239 outlines the image analysis steps. The phase
240 information enables the determination of the
241 refractive index of the sample. As a result,
242 knowing the concentration derivative of the
243 refractive index ($\partial n/\partial c$) is possible to
244 determine the entire concentration profile
245 along the micro-column for each instant (for
246 each acquired image). Once the mixture
247 reach the stationary stage, the slope of the
248 concentration along the height of the micro-
249 column ($\partial c/\partial z$) is used in order to
250 determine the thermodiffusion coefficient.

251 This concentration profile correspond to the
 252 midline of y scale of the column in y-z plane

253 (bounded by white dashed lines in Fig.4).

254



255

256

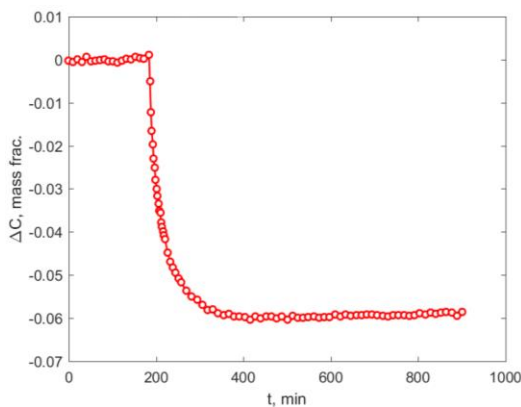
Fig.4 Steps for the phase information extraction of each acquired image.

257

258 The concentration variation during the all
 259 experiment is shown in Fig.5. There it can
 260 be appreciate the stabilization process at
 261 25°C for approximately 3-4 hours. Then, the
 262 temperature gradient is applied so
 263 concentration in the sample start changing
 264 until mixture reach the stationary state.
 265 Negative concentration variation means that
 266 the reference component is enriched at the
 267 bottom part of the micro-column.

272 3. Results and discussion

273 For the validation of the new analysis
 274 method, we have measured the
 275 thermodiffusion coefficients of three binary
 276 mixtures at equal mass fraction of THN
 277 (purity, 98+%), IBB (purity, 99%) and C12
 278 (purity, 99%). All measurements have been
 279 carried out at mean temperature of 25°C.
 280 The thermophysical properties as density,
 281 thermal expansion and dynamic viscosity
 282 were taken from (Alonso de Mezquia et al.
 283 2015) and the contrast factor $(\partial n / \partial c)$ at 633
 284 nm wavelength of three binary mixtures was
 285 taken from (Gebhardt et al. 2013). To
 286 calculate the $(\partial n / \partial c)$ at 470 nm, Cauchy
 287 dispersion relation has been used as it is
 288 detailed in (Mialdun, A. and Shevtsova
 289 2017). In Table 1, all the optical and
 290 thermophysical properties taken from
 291 literature are shown.



268

269 Fig.5 Time evolution of the concentration separation
 270 of THN-C12 binary mixture at 50% of mass fraction
 271 with $\Delta T = 8^\circ C$, monitored by 470nm wavelength.

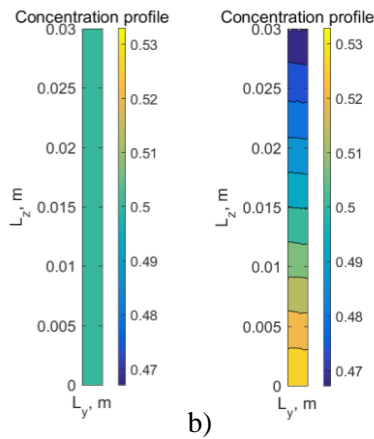
292 Table 1. Optical and thermophysical properties of
 293 THN-IBB-C12 binary mixtures at equal mass fraction
 294 at 25°C. Density, thermal expansion and dynamic

295 viscosity are taken from (Alonso de Mezquia et al.
 296 2015) and $(\partial n/\partial c)$ from (Gebhardt et al. 2013).

	THN- C12	THN- IBB	IBB- C12
ρ (kg/m^3)	841.248	904.514	792.355
$\alpha \times 10^{-3}$ (K^{-1})	0.895	0.888	0.961
$\mu \times 10^{-3}$ ($Pa \cdot s$)	1.523	1.374	1.133
$(\partial n/\partial c)$ ($\lambda = 633nm$)	0.1155	0.0547	0.0625
$(\partial n/\partial c)$ ($\lambda = 470nm$)	0.1258	0.0577	0.0700

297

298 During the image processing, the
 299 concentration in the entire cross-section of
 300 the cell is determined from each image. The
 301 Fig.6a shows the initial concentration
 302 profile when the micro-column is stabilized
 303 at $25^\circ C$ and in Fig.6b when it reaches the
 304 stationary state with $\Delta T = 8^\circ C$.

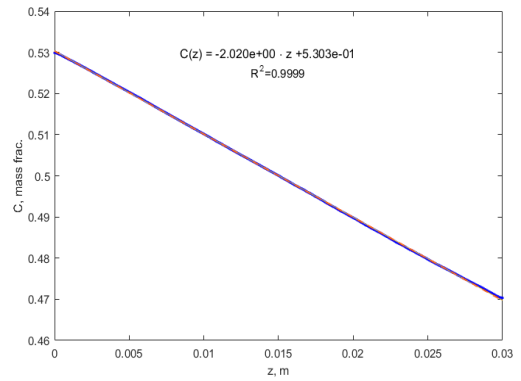


305 a)

b)

306 Fig.6 Concentration profiles inside the micro-column
 307 filled with THN-C12 at 50 % mass fraction; a) when
 308 mixtures is stabilized at $25^\circ C$, b) when the mixture
 309 reaches the stationary state after applying $\Delta T = 8^\circ C$.

310 Afterwards, the vertical concentration
 311 profile is represented in function of the
 312 height of the micro-column and is fitted with
 313 the polynomial of the first order obtaining
 314 $(\partial c/\partial z)$ as shown in Fig.7.



315

316 Fig.7 Concentration gradient at stationary state along
 317 the height of the micro-column of THN-C12 at 50%
 318 mass fraction with $\Delta T = 8^\circ C$.

319 Finally, the thermodiffusion coefficient of
 320 binary mixtures is determined (4) (Larrañaga
 321 et al. 2014),

$$D_T = -\frac{L_x^4}{504 \nu C_0} \frac{g \alpha}{(1-C_0)} \frac{\partial c}{\partial z} \quad (4)$$

322 where, L_x is the gap of the micro-column,
 323 g is the gravity, α is the thermal expansion
 324 coefficient, ν is the kinematic viscosity and
 325 C_0 is the initial concentration of the
 326 reference component.

327 The Table 2, Table 3 and Table 4 show the
 328 thermodiffusion coefficients of THN-C12,
 329 THN-IBB and IBB-C12 binary mixtures and
 330 the mean values with the respective
 331 deviations.

332 The obtained results show a good agreement
 333 with Benchmark Fontainebleau values
 334 (Platten et al. 2003) that makes us confident
 335 in reliability of the new configuration.

336 For the first time, with the new
 337 configuration, we have analysed all the
 338 height of the column and we have seen the
 339 entire concentration profile inside the
 340 thermogravitational column.

341 Table 2. Thermodiffusion coefficients of THN-C12 binary mixtures at 50% mass fraction.

THN-C12	633 nm		470 nm		Benchmark (Platten et al. 2003)
	$(\partial c/\partial z)$	$D_T \times 10^{-12}$ (m^2/sK)	$(\partial c/\partial z)$	$D_T \times 10^{-12}$ (m^2/sK)	
1	-2.124	5.53	-2.070	5.39	
2	-2.264	5.90	-2.177	5.66	
3	-2.304	5.99	-2.275	5.92	
4	-2.260	5.88	-2.180	5.68	
5	-2.299	5.99	-2.212	5.76	
Average	-2.250	5.86±0.33	-2.183	5.68±0.29	5.9±0.3

342

343 Table 3. Thermodiffusion coefficients of THN-IBB binary mixtures at 50% mass fraction.

THN-IBB	633 nm		470 nm		Benchmark (Platten et al. 2003)
	$(\partial c/\partial z)$	$D_T \times 10^{-12}$ (m^2/sK)	$(\partial c/\partial z)$	$D_T \times 10^{-12}$ (m^2/sK)	
1	-1.062	3.27	-1.010	3.11	
2	-0.801	2.46	-0.794	2.44	
3	-0.844	2.60	-0.804	2.68	
4	-1.062	3.27	-0.983	3.03	
5	-0.937	3.03	-0.984	2.89	
6	-0.902	2.78	-0.877	2.70	
Average	-0.935	2.90±0.44	-0.909	2.81±0.37	2.8±0.1

344

345 Table 4. Thermodiffusion coefficients of IBB-C12 binary mixtures at 50% mass fraction.

IBB-C12	633 nm		470 nm		Benchmark (Platten et al. 2003)
	$(\partial c/\partial z)$	$D_T \times 10^{-12}$ (m^2/sK)	$(\partial c/\partial z)$	$D_T \times 10^{-12}$ (m^2/sK)	
1	-1.079	3.82	-1.022	3.61	
2	-0.994	3.52	-0.987	3.49	
3	-1.209	4.28	-1.094	3.87	
4	-1.123	3.98	-1.074	3.80	
5	-1.146	4.06	-1.112	3.94	
6	-1.071	3.79	-0.988	3.49	
Average	-1.104	3.91±0.39	-1.046	3.70±0.24	3.7±0.2

346

347 4. Conclusions

348 In this work, we have changed the
 349 configuration of the previously reported
 350 optical analysis method applied to
 351 thermogravitational micro-column. The new
 352 configuration of the interferometer and the
 353 image processing is based on Optical Digital
 354 Interferometry analysis method. With the
 355 new configuration, we are able to analyse
 356 the entire window of micro-column instead
 357 of analysing only two points. Thanks to this
 358 improvement, we are able to see the entire
 359 concentration profile inside the micro-
 360 column during the measurements.

361 To validate the new system, we have
 362 determined the thermodiffusion coefficients
 363 of three binary mixtures at equal mass
 364 fractions. Results have been compared with
 365 Benchmark Fontainebleau

366 The new analysis method can be readily
 367 extended to analyse ternary mixtures. The
 368 analysis of the entire concentration profile
 369 will allow to study the thermogravitational
 370 effect in the transitory state of binary and
 371 ternary mixtures.

372 Acknowledgements

373 Authors would like to thank the support of
374 Research Groups (IT1009-16) and Research
375 Fellowship (Pre_2014_1_283) of Basque
376 Government, TERDISOMEZ (FIS2014-
377 58950-C2-1-P) and MEZNAFLU
378 (ESP2017-83544-C3-1-P) of the MINECO
379 and DCMIX (DCMIX-NCR-00022-QS)
380 from the European Space Agency. Also
381 would like to thank Denatek engineering and
382 manufacturing technology company for
383 manufacturing the gap.

384 References

385 Alonso de Mezquia, D., Larrañaga, M., Bou-Ali,
386 M.M., Madariaga, J.A., Santamaría, C., Platten, J.K.:
387 Contribution to thermodiffusion coefficient
388 measurements in DCMIX project. *Int. J. Therm. Sci.*
389 92, 14–16 (2015).
390 doi:10.1016/j.ijthermalsci.2015.01.013

391 Gebhardt, M., Köhler, W., Mialdun, A., Yasnou, V.,
392 Shevtsova, V.: Diffusion, thermal diffusion, and Soret
393 coefficients and optical contrast factors of the binary
394 mixtures of dodecane, isobutylbenzene, and 1,2,3,4-
395 tetrahydronaphthalene. *J. Chem. Phys.* 138, 114503
396 (2013). doi:10.1063/1.4795432

397 Kolodner, P., Williams, H., Moe, C.: Optical
398 measurement of the Soret coefficient of ethanol/water
399 solutions. *J. Chem. Phys.* 88, 6512–6524 (1988)

400 Larrañaga, M., Bou-Ali, M.M., Lapeira, E.,
401 Santamaría, C., Madariaga, J.A.: Effect of
402 Thermophysical Properties and Morphology of the
403 Molecules on Thermodiffusion Coefficient of Binary
404 Mixtures. *Microgravity Sci. Technol.* 26, 29–35
405 (2014). doi:10.1007/s12217-014-9368-y

406 Larrañaga, M., Bou-Ali, M.M., Lizarraga, I.,
407 Madariaga, J.A., Santamaría, C.: Soret coefficients of
408 the ternary mixture 1,2,3,4-tetrahydronaphthalene +
409 isobutylbenzene + n-dodecane. *J. Chem. Phys.* 143,
410 24202 (2015)(a). doi:10.1063/1.4926654

411 Larrañaga, M., Bou-Ali, M.M., Lizarraga, I.,
412 Madariaga, J.A., Santamaría, C.: Soret coefficients of
413 the ternary mixture 1,2,3,4-tetrahydronaphthalene +
414 isobutylbenzene + n-dodecane. *J. Chem. Phys.* 143,
415 24202 (2015)(b). doi:10.1063/1.4926654

416 Mialdun, A. and Shevtsova, V.: Analysis of multi-
417 wavelength measurements of diffusive properties via
418 dispersion dependence of optical properties. *Appl.*
419 *Opt.* 56, 572–581 (2017)

420 Mialdun, A., Legros, J.-C., Yasnou, V., Sechenyh, V.,
421 Shevtsova, V.: Contribution to the benchmark for
422 ternary mixtures: Measurement of the Soret, diffusion
423 and thermodiffusion coefficients in the ternary mixture
424 THN/IBB/nC12 with 0.8/0.1/0.1 mass fractions in
425 ground and orbital laboratories. *Eur. Phys. J. E.* 38, 27
426 (2015). doi:10.1140/epje/i2015-15027-2

427 Mialdun, A., Shevtsova, V.: Measurement of the
428 Soret and diffusion coefficients for benchmark binary
429 mixtures by means of digital interferometry. *J. Chem.*
430 *Phys.* 134, 44524 (2011). doi:10.1063/1.3546036

431 Mialdun, A., Shevtsova, V.M.: Development of
432 optical digital interferometry technique for
433 measurement of thermodiffusion coefficients. *Int. J.*
434 *Heat Mass Transf.* 51, 3164–3178 (2008).
435 doi:10.1016/j.ijheatmasstransfer.2007.08.020

436 Naumann, P., Martin, A., Kriegs, H., Larrañaga, M.,
437 Bou-Ali, M.M., Wiegand, S.: Development of a
438 thermogravitational microcolumn with an
439 interferometric contactless detection system. *J. Phys.*
440 *Chem. B.* 116, 13889–97 (2012).
441 doi:10.1021/jp3098473

442 Platten, J.K., Bou-Ali, M.M., Costesèque, P.,
443 Dutrieux, J.F., Köhler, W., Leppla, C., Wiegand, S.,
444 Wittko, G.: Benchmark values for the Soret, thermal
445 diffusion and diffusion coefficients of three binary
446 organic liquid mixtures. *Philos. Mag.* 83, 1965–1971
447 (2003). doi:10.1080/0141861031000108204

448 Urteaga, P., Bou-Ali, M.M., Alonso De Mezquia, D.,
449 Santamaría, J., Santamaría, C., Madariaga, J.A.,
450 Bataller, H.: Measurement of thermodiffusion
451 coefficient of hydrocarbon binary mixtures under
452 pressure with the thermogravitational technique. *Rev.*
453 *Sci. Instrum.* 83, (2012). doi:10.1063/1.4737628

454 Wiegand, S., Ning, H., Kriegs, H.: Thermal diffusion
455 forced Rayleigh scattering Setup optimized for
456 aqueous mixtures. *J. Phys. Chem. B.* 111, 14169–
457 14174 (2007). doi:10.1021/jp076913y

458 Wittko, G., Köhler, W.: Precise determination of the
459 Soret, thermal diffusion and mass diffusion
460 coefficients of binary mixtures of dodecane,
461 isobutylbenzene and 1,2,3,4-tetrahydronaphthalene by
462 a holographic grating technique. *Philos. Mag.* 83,
463 1973–1987 (2003).
464 doi:10.1080/0141861031000108213

465 Zhang, K.J., Briggs, M.E., Gammon, R.W., Sengers,
466 J. V.: Optical measurement of the Soret coefficient
467 and the diffusion coefficient of liquid mixtures. *J.*
468 *Chem. Phys.* 104, 6881 (1996). doi:10.1063/1.471355

469